Article

1D Zn(II) Coordination Polymers as Effective Heterogeneous Catalysts in Microwave-Assisted Single-Pot Deacetalization-Knoevenagel Tandem Reactions in Solvent-Free Conditions

Anup Paul *, Anirban Karmakar, M. Fátima C. Guedes da Silva and Armando J. L. Pombeiro *

Centro de Química Estrutura, Instituto Superior Técnico, Universidade de Lisboa, Avenida Rovisco Pais, 1049-001 Lisboa, Portugal; anirban.karmakar@tecnico.ulisboa.pt (A.K.); fatima.guedes@tecnico.ulisboa.pt (M.F.C.G.d.S.)

* Correspondence: anuppaul@tecnico.ulisboa.pt (A.P.); pombeiro@ist.utl.pt (A.J.L.P.)

Abstract: The new 1D CPs $[Zn(L^1)(H_2O)_4]_n \cdot nH_2O$ (**1**) and $[Zn(L^2)(H_2O)_2]_n$ (**2**) [L^1 = 1,1'-(ethane-1,2-diyl)bis(6-oxo-1,6-dihydropyridine-3-carboxylic acid); L^2 = 1,1'-(propane-1,3-diyl)bis(6-oxo-1,6-dihydropyridine-3-carboxylic acid)] were prepared from flexible dicarboxylate pro-ligands (H_2L^1 and H_2L^2). Both CPs **1** and **2** were characterized by elemental, FTIR, and powder X-ray diffraction analysis. Their geometry and the structural features were unveiled by single-crystal X-ray diffraction analysis. The underlying topology of the CPs was illustrated by the topological analysis of the H-bonded structure of CP **1**, which revealed a 3,4,6-connected trinodal net. On the other hand, topological analysis on the hydrogen-bonded network of CP **2** showed a 2,3,3,4,6,7-connected hexanodal net. The thermal stability of the CPs was investigated by thermogravimetric analysis. CPs **1** and **2** act as heterogeneous catalysts in one-pot tandem deacetalization–Knoevenagel condensation reactions under environmentally mild conditions. CPs **1** exhibits a yield of ca. 91% in a microwave-assisted solvent-free medium, whereas a slightly lower yield was obtained for CP **2** (87%) under the same experimental protocol. The recyclability of catalyst **1** was also assessed. To our knowledge, these are the first Zn(II)-based CPs to be applied as heterogeneous catalysts for the above tandem reactions under environmentally friendly conditions.

Keywords: coordination polymers; heterogeneous catalyst; tandem reactions; microwave; solvent-free

1. Introduction

Coordination polymers (CPs) have attracted an enormous interest over the years not only because of their intriguing architectures and topologies, but also for their diversified applications in various areas such as gas adsorption and separation, molecular magnetism, luminescence, sensing, etc. [1–7]. Apart from these, CPs, as heterogeneous catalysts have also marked their foothold due to their recyclability and easy workup [8–13]. Numerous factors such as the choice of organic ligands, metal ions, solvent, metal to ligand ratio, pH, temperature, etc. play a crucial role in the self-assembly processes of CPs [14,15]. In the design of CPs, the rigid ligands have mostly been accounted for as a well-known way to generate multidimensional structures [16–20]. On the other hand, it is hard to develop CPs with flexible ligands due to their flexible nature, which can adopt different orientations during the self-assembly process [21–24]. Nevertheless, the conformational opportunity of the flexibly adaptable ligands offers a greater possibility for the development of multidimensional structures with uncommon topological and microporous CPs [25–28]. Among the different organic linkers, flexible multicarboxylate (in particular dicarboxylate) ligands have been regularly employed as multifunctional linkers in light of their plentiful coordination modes to a metal ion for the generation of polymeric frameworks.

For example, dicarboxylic acids such as succinic acid, glutaric acid, adipic acid, etc. are the sorts of carboxylic acids that have been chosen to construct multidimensional structures because of the presence of a flexible C–C bond [29,30]. Dicarboxylate ligands with a flexible C–C bond can be viewed as a convenient linker for the construction of multidimensional CPs. Keeping these concepts in mind, two new pro-ligands (Figure 1) have been designed having both a dicarboxylate linker and a flexible C–C arm for the construction of CPs.
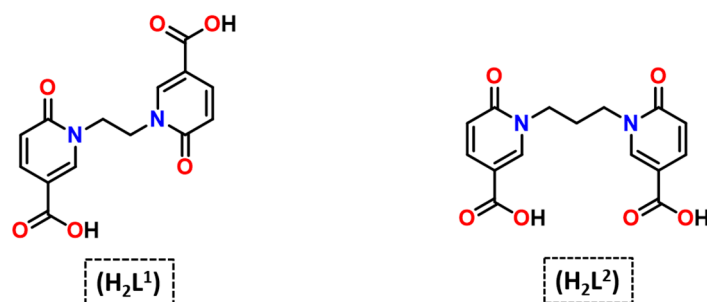

**Figure 1.** Structure of pro-ligands H_2L^1 and H_2L^2.

Concerning catalysis, an array of CPs have been developed as heterogeneous catalysts for various organic transformations [9–13]. In contrast with homogeneous catalysts, the heterogeneous ones have favorable recompences due to their easy separation and recyclability. Amongst the various metal-based CPs in catalysis, Zn(II) CPs as heterogeneous catalysts have gained a noteworthy consideration over the years [13,31–34]. For instance, we have reported a few amide functionalized Zn(II) MOFs that can be applied in different catalytic responses, for example, Knoevenagel condensation, cyanosilylation, and Henry reactions [35–38]. Moreover, in the domain of catalysis, tandem reactions, in which two or more individual reactions are accomplished in a single pot, are of high demand due to their reduced energy consumption and reaction time, aside from avoiding the excess utilization of solvents and chemicals [39,40]. The deacetalization–Knoevenagel condensation is one of the exciting examples of one-pot cascade reactions, wherein benzylidene malononitrile is obtained straightforwardly by utilizing benzaldehyde dimethyl acetal and malononitrile [41,42]. MOF catalysts with both Lewis acidic and basic sites have been documented for such types of reaction [41–46]. Nevertheless, in almost all cases, an organic medium was used for carrying out the reaction, and there has been hardly been any reports on efficient heterogeneous MOFs/CPs as catalysts for such reactions carried out under environmentally friendly solvent-free conditions. Furthermore, a main barrier associated with the design of such a type of catalyst for those reactions concerns the possible neutralization of the effects of the acidic and basic moieties.

Hence, intending to discover new heterogeneous catalysts, herein we present two new Zn(II) 1D CPs bearing acidic and basic sites, $[Zn(L^1)(H_2O)_4]_n \cdot nH_2O$ (**1**) and $[Zn(L^2)(H_2O)_2]_n$ (**2**), with flexible multicaboxylate ligands and their application as environmentally friendly heterogeneous catalysts for solvent-free microwave-assisted one-pot deacetalization–Knoevenagel condensation tandem reactions.

2. Results and Discussion

2.1. Syntheses and Characterization

The pro-ligands 1,1′-(ethane-1,2-diyl)bis(6-oxo-1,6-dihydropyridine-3-carboxylic acid) (H_2L^1) and 1,1′-(propane-1,3-diyl)bis(6-oxo-1,6-dihydropyridine-3-carboxylic acid) (H_2L^2) were synthesized by treating methyl 6-hydroxyisonicotinate with 1,2-dibromoethane (for H_2L^1) and 1,3-dibromopropane (for H_2L^2) in the presence of K_2CO_3 in acetone under stirring at room temperature followed by hydrolysis, as presented in Scheme S1, ESI. The coordination polymers **1** and **2** were prepared by the hydrothermal reaction of H_2L^1 and H_2L^2 with $Zn(NO_3)_2 \cdot 6H_2O$, respectively, in a solvent mixture of DMF:H_2O at 80 °C for 48 h as depicted in Scheme 1.
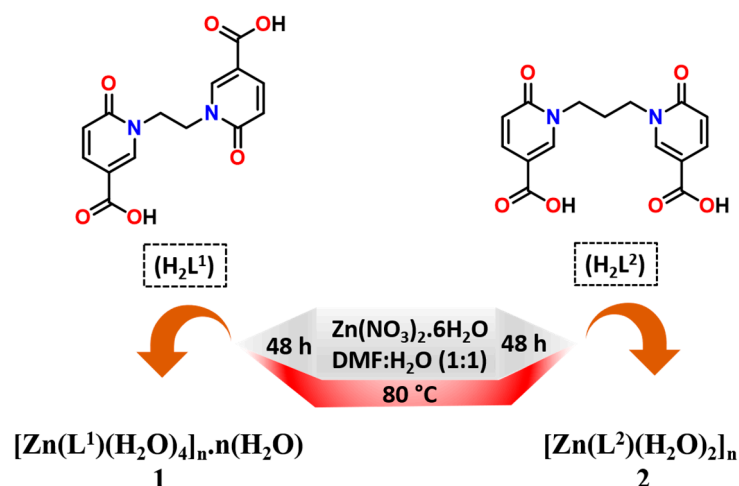
Scheme 1. Syntheses of CPs **1** and **2**.

The pro-ligands H_2L^1 and H_2L^2 were characterized by elemental analyses, infrared, ^{1}H, and ^{13}C NMR techniques. On the other hand, the derived CPs **1** (from H_2L^1) and **2** (from H_2L^2) were characterized by elemental analysis, infrared, and thermogravimetric analyses. Furthermore, geometrical and structural aspects of the CPs **1** and **2** were revealed by single-crystal diffraction analysis (outlined below). Both pro-ligands H_2L^1 and H_2L^2 exhibited trademark resonances due to –COO(H) at δ 12.81 in their ^{1}H-NMR spectra (Figures S1 and S2). The resonance due to –CH$_2$ protons was observed at δ 4.31 for H_2L^1 and at δ 4.01 and 2.04 for H_2L^2. The aromatic proton resonances were shown in the range of δ 8.49–6.35. The ^{13}C NMR spectrum of H_2L^1 (Figure S3) and H_2L^2 (Figure S4) exhibited a resonance at δ 165.79 and 164.89, respectively, due to –$\underline{C}$OOH. The signals due to two –$\underline{C}$H$_2$– carbons in the case of H_2L^1 were noticed at δ 47.22 and 29.26, whereas, for H_2L^2, three different signals were spotted at δ 52.18, 47.26, and 28.63, respectively, for the three –$\underline{C}$H$_2$– carbons.

The ν(COO) characteristic vibration bands in the IR spectra of the pro-ligands H_2L^1 and H_2L^2 were observed at 1697 and 1708 cm^{-1}, respectively (Figure S5). On the other hand, in the IR spectra of the CPs, the intensive vibration observed at ca. 1562 cm^{-1} (for **1**) and 1552 cm^{-1} (for **2**), along with a medium intensity band at ca. 1416 cm^{-1} for both CPs, were assigned to the νCO$_{asym}$ and νCO$_{sym}$ vibrations, respectively (Figure S5). The alteration of the characteristic vibrations concerning the free carboxylate of the pro-ligands indicates the coordination to zinc(II) centers, as further demonstrated by single-crystal X-ray diffraction analysis as discussed below. Furthermore, powder-XRD was additionally performed. The experimental and simulated PXRD patterns showed that the materials were of an identical sort (Figures S6 and S7).

2.2. Crystal Structure Analysis of **1** and **2**

According to the single X-ray diffraction analysis, both CPs [Zn(L)(H$_2$O)$_4$]$_n$.nH$_2$O (**1**) and [Zn(L)(H$_2$O)$_2$]$_n$ (**2**) had one-dimensional structures. The CP **1** had a 1D network with an asymmetric unit made of two Zn^{2+} ions (each of them with an 0.5 occupancy), one (L^1)$^{2-}$ ligand, four water ligands (two per metal cation), and one non-coordinated water molecule (Figure 2A). Symmetry expansion revealed that both the Zn(II) centers had octahedral coordination geometry. The Zn1 center was coordinated by two carboxylate-O from two (L^1)$^{2-}$ ligands [Zn1-O1 1.961(5) Å] and four water molecules [Zn1-O7A 2.074(13) and Zn1-O8A 2.143(14)], whereas the coordination environment of the Zn2 center was fulfilled by two keto-O atoms from two neighboring (L^1)$^{2-}$ ligands [Zn2-O3 2.073(8) Å] and four water molecules [Zn2-O9 2.153(8) and Zn2-O10 2.063(8)] (Figure 2B). The Zn-O$_{water}$ bond distances were in the range of 2.063 Å to 2.163(17) Å. Since in **1**, the Zn1 and Zn2 centers are attached to the same pyridine ring, they alternate their positions to create the 1D

linear chain-like structure (Figure 2C). The carboxylate and keto groups from the remaining pyridine ring are uncoordinated and only participate in H-bonding interactions. In CP **1**, the organic ligand adopts a stair type orientation with the pyridine rings residing in two different and almost parallel planes (bit angle of 3.24°) and the N1-C7-C8-N2 torsion angle of 169.73°. The plane of the carboxylate group is approximately in the pyridine plane (bite angle of 7.93°). The Zn···Zn distance is 10.158 Å.

(**A**)

(**B**)
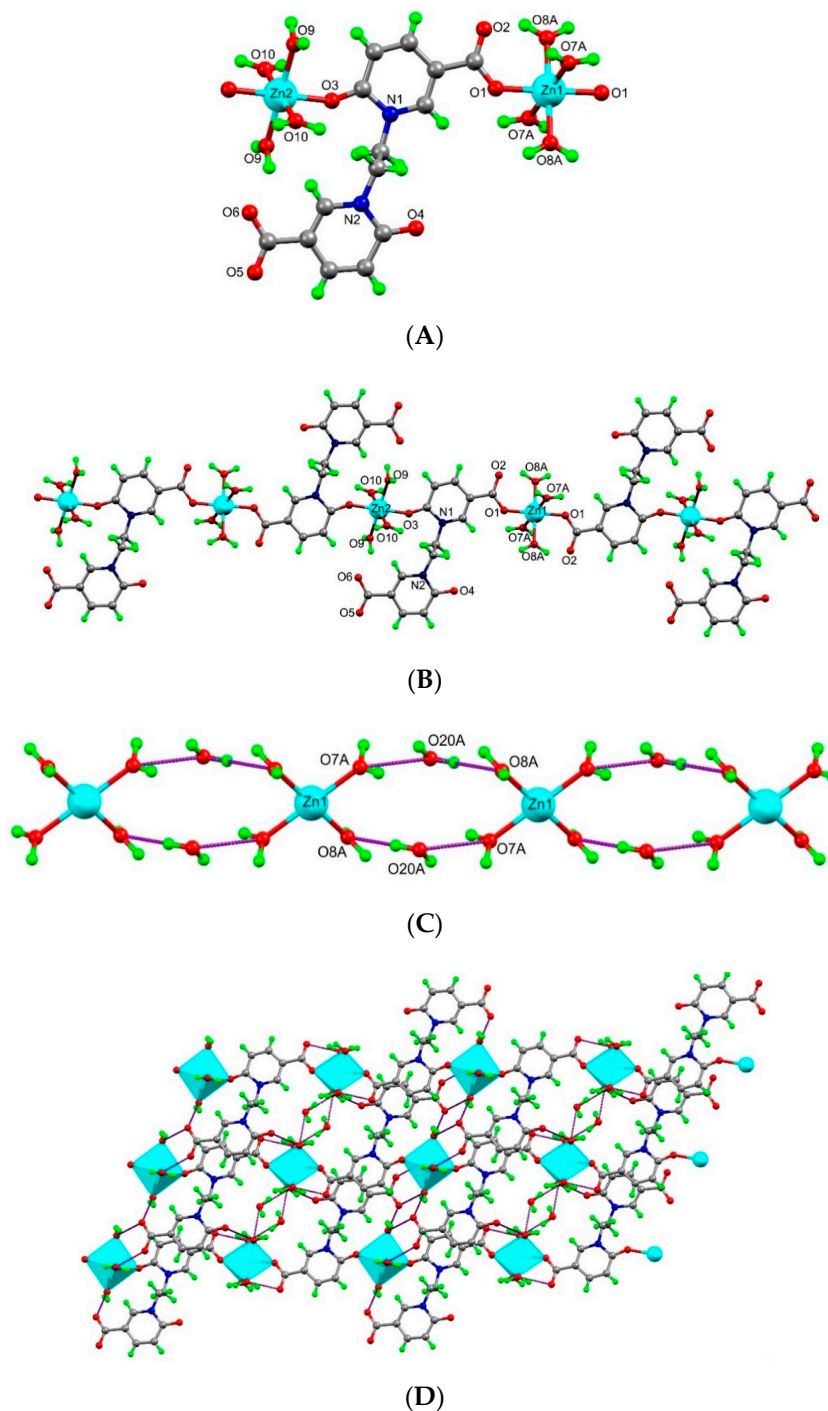
(**C**)

(**D**)

Figure 2. (**A**) The structure of CP **1** with partial atom labelling scheme. (**B**) One dimensional linear structure of CP **1**. (**C**) 1D hydrogen bonded double chain constructed by [Zn(H$_2$O)$_4$] and a non-coordinated water molecule. (**D**) Three-dimensional hydrogen bonded network in CP **1** (the hydrogen bonding interactions are indicated as purple lines).

As shown in Figure 2D, the presence of widespread H-bond interactions was observed in CP **1**, and the most relevant ones are presented in Table S2. The important bond distances and angles of CP **1** are depicted in Table S3. Furthermore, in CP **1**, the uncoordinated carboxylates (O5 and O6) and keto (O4) groups act as hydrogen acceptors and the coordinated water molecules (O7A, O9 and O10) as hydrogen donors. The $[Zn(H_2O)_4]$ unit is hydrogen-bonded with the non-coordinated water molecule in such a way that it generates a one-dimensional double chain, as shown in Figure 2D. Several O–H⋯O and C–H⋯O interactions are present in the structure of **1**, which help to expand the structure to a third dimension H-bonded network.

The asymmetric unit of **2** contains one deprotonated ligand $(L^2)^{2-}$, one Zn(II) cation, and two coordinated water molecules (Figure 3A). Symmetry expansion revealed the Zn(II) metal center with a tetrahedral geometry $(\tau_4 = 0.81)$[1] where the coordination sphere occupied with two carboxylate oxygen atoms from two $(L^2)^{2-}$ ligands and two oxygen atoms from two water molecules. The combination of Zn(II) ions and $(L^2)^{2-}$ ligands form a zig-zag type 1D framework, which is shown in Figure 3B.
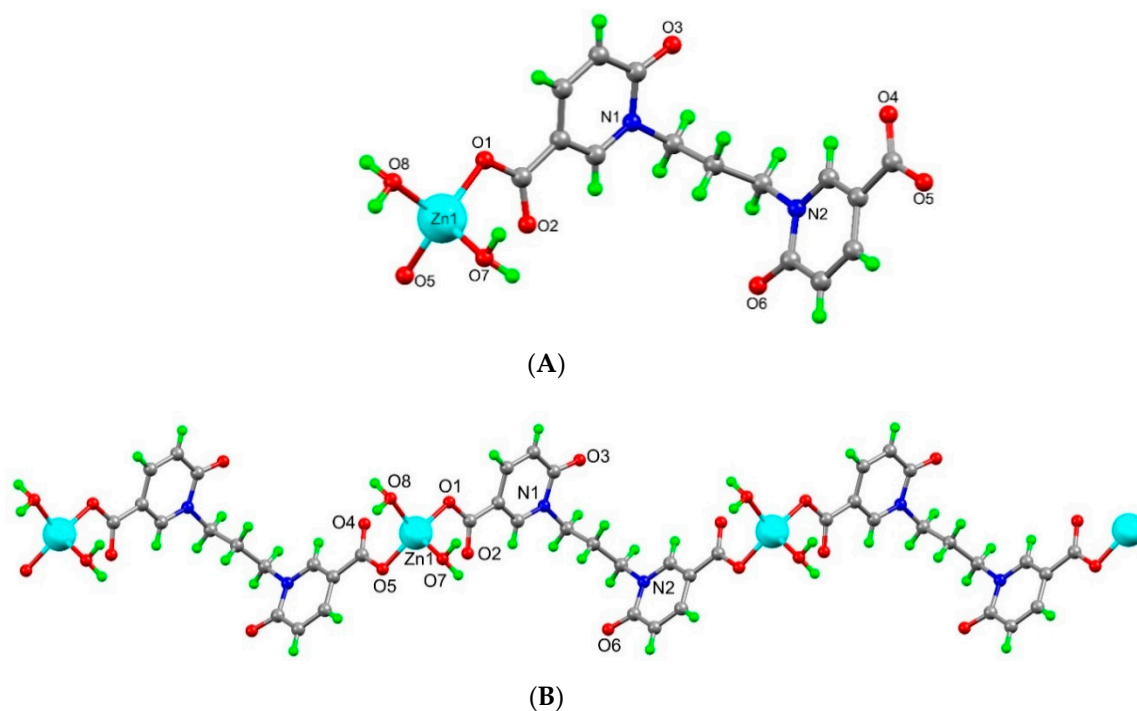

(**A**)

(**B**)

Figure 3. (**A**) The structure of framework **2** with the partial atom labelling scheme. (**B**) One dimensional *zig-zag* structure of framework **2**.

The Zn-O bond lengths were in the range of 1.960(6)–2.020(6) Å and the O–Zn–O bond angles were between 99.8(2)° and 107.5(3)°. The Zn⋯Zn distance between the two-symmetry related metal centers is 13.784(3) Å. Selected bond distances and angles of **2** are listed in Table S3 (Supplementary Materials). In this framework, the organic ligand has a "W" type orientation and the angle between the two pyridine rings is 89.02°. Both the carboxylate groups of $(L^2)^{2-}$ are coordinated to Zn(II) ions in a monodentate fashion and reside almost in the planes of the respective pyridine rings (bite angles of 11.01° and 13.47°). The C2-C1-O1-Zn1 and C13-C14-O5-Zn1′ torsion angles were −178.77° and −179.52°, respectively. The keto groups of $(L^2)^{2-}$ were not coordinated to the Zn(II) center, but they participate in hydrogen bonding interactions with coordinated water molecules involving O7-H6O⋯O2 [$d_{D–A}$ 2.779(9) Å; < D–H⋯A 179°], O7-H7O⋯O3 [$d_{D–A}$ 2.615(9) Å; < D–H⋯A 178°], O8-H8O⋯O4 [$d_{D–A}$ 2.782(8) Å; < D–H⋯A 179°], and O8-H9O⋯O(6) [$d_{D–A}$ 2.620(10) Å; < D–H⋯A 179°] interactions and form a two-dimensional H-bonded network.

Moreover, this 2D hydrogen-bonded network is further assembled via various C–H···O interactions, generating a three-dimensional structure with ca. 8.1 Å × 8.9 Å rectangular voids along the *bc*-plane (Figure 4).
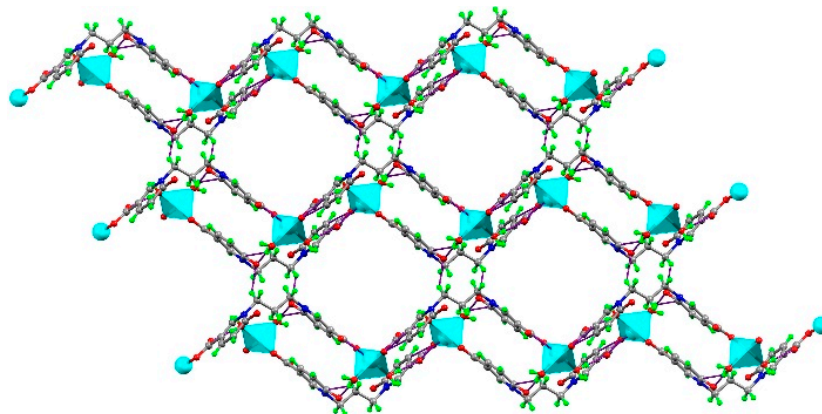

Figure 4. Three-dimensional hydrogen-bonded network of CP **2**.

2.3. Topological Analysis of **1** and **2**

We performed the topological analysis of the hydrogen-bonded networks of **1** and **2** by reducing its multidimensional structure to simple node-and-linker net[1] using software TOPOS 4.0.17 [47–49]. The topological analysis of the H-bonded structure of compound **1** revealed that it has a 3,4,6-connected trinodal net and point symbol $\{4.6^4.8\}\{4^2.6^8.8^5\}\{4^3\}_2$, whereas the hydrogen-bonded network of compound **2** exhibits a more complex 2,3,3,4,6,7-connected hexanodal net with point symbol $\{3.4^2\}_2\{3.4^3.5^2.6^7.7^3.8^5\}_2\{3^2.4^2.5^2.6^4.7^4.9\}$ $\{4^2.6\}_2\{6^4.8.10\}\{6\}_2$ (Figure 5A,B).

(**A**)   (**B**)
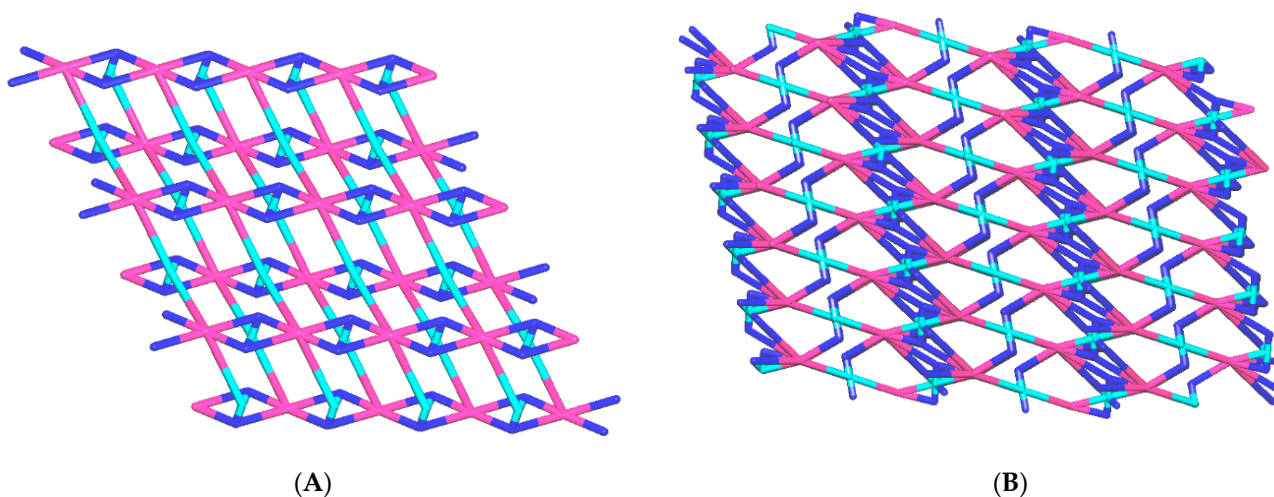
Figure 5. Node-and-linker-type descriptions of the 2D hydrogen bonded networks of CP **1** (**A**) and **2** (**B**). Metal node as cyan, ligand as pink and hydrogen bonding interactions are indicated as blue color.

2.4. Thermogravimetric Analysis of **1** and **2**

Thermogravimetric analyses (TGA) of the CPs **1** and **2** were examined to see their thermal stabilities in the temperature range of 30–800 °C with a heating rate of 10 °C min^{-1} under a dinitrogen atmosphere. As depicted in Figure 6, CP **1** exhibited a weight loss of 3.85% in the temperature range of ca. 80–100 °C, resulting from the loss of one lattice water molecule (calculated = 3.93%). A further step with a weight loss of ca. 15.2% (calculated = 15.73%) was detected in the temperature range of ca. 100–140 °C, accountable

for the loss of the four coordinated water molecules. At ca. 140–330 °C it was stable, but over 330 °C, the polymeric framework deteriorated, prompting the generation of ZnO. On the other hand, CP **2** displayed a sharp decay in its TGA curve (Figure 6) in the range of ca. 65–105 °C in conjunction with the weight loss of ca. 8.1% (calcd. 7.93%), responsible for the loss of two lattice water molecules. An immediate second step with a weight loss of ca. 7.8% (calcd. 7.93%) was detected in the temperature range of 105–175 °C due to the loss of the two coordinated water molecules. It was then found to be thermally stable up to 300 °C, beyond which it breaks down to produce ZnO.
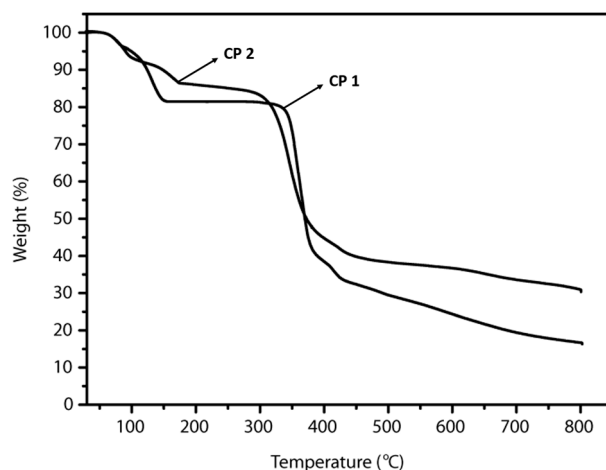

Figure 6. Thermogravimetric analysis of CPs **1** and **2**.

2.5. Catalytic Activity

Taking advantage of the thermal robustness of CPs **1** and **2** and their insolubility in most of the common organic solvents, they were tested for the one pot deacetalization-Knoevenagel reaction as heterogeneous catalysts (Scheme 2). As mentioned earlier, the advantage of the one-pot tandem reactions lies where two subsequent reactions can be completed in one step. In the first part, benzaldehyde (B) is produced from benzaldehyde dimethyl acetal (A), and the subsequent reaction concerns the conversion of B to benzylidene malononitrile (C) in the presence of malononitrile through a Knoevenagel condensation. The former reaction is usually triggered by the presence of a Lewis acid in the framework, while the latter is promoted by a Lewis base. The developed CPs **1** and **2** satisfy the perquisite of displaying a Zn(II) metal ion, which can act as a Lewis acid, and basic sites such as pyridyl-N and oxygen-O, which are favorable for engaging them as catalysts in the tandem reaction.
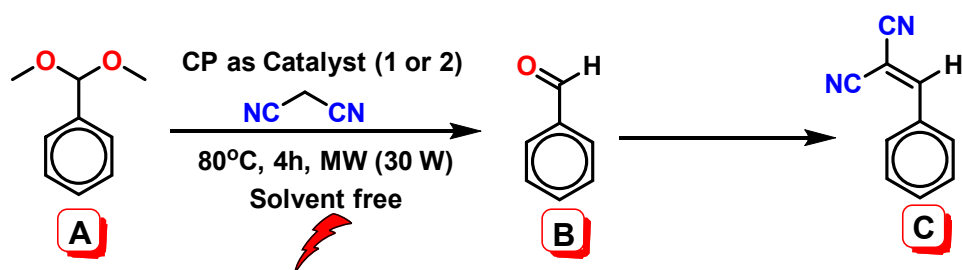
Scheme 2. One-pot deacetalization-Knoevenagel condensation reactions, benzaldehyde dimethyl acetal (**A**), benzaldehyde (**B**) and benzylidene malononitrile (**C**).

Thus, to explore such a possibility, microwave irradiation (MW) was applied as a well-known technique that can accelerate the reaction and generate higher yield and selectivity.

Our group, along with other established research groups, are actively involved in using the MW technique for several catalytic transformations [36,50–52].

Under typical conditions, a combination of the initial reagent benzaldehyde dimethyl acetal (A, 0.152 g, 1.0 mmoL), with the methylene activated one (i.e., malononitrile (0.132 g, 2.0 mmoL) and the zinc CP catalyst (15.2 mg or 27.0 mg for **1** or **2**, respectively; 3.0 mol%)) was placed in a glass vessel covered with a Teflon cap and stirred at 80 °C under microwave irradiation (30 W) for 4 h in solvent-free conditions. The desired product was identified by ^{1}H NMR spectroscopy (Figures S1 and S8).

The catalysts were screened in the absence and presence of different solvents, upon varying temperature (25–100 °C), catalyst loading (1–5 mol%), and reaction time (up to 4 h) to optimize the reaction conditions under MW heating.

Among the tested solvents viz., DMF, CH$_3$CN, DMSO, and THF, the maximum obtained yield was in DMF (47% yield for **1**), followed by DMSO (45% yield for **1**), THF (32% yield for **1**), and CH$_3$CN (21% yield for **1**) at 80 °C after 4 h under MW irradiation (Table 1, entries 8–10). However, the best yield was obtained when the reaction was carried out in a solvent-free medium under the same optimized condition (91% yield for **1** and 87% yield for **2**) (Table 1, entries 1 and 2). The study uncovered that both CPs **1** and **2** exhibited comparable catalytic activities, although the former were more active, which may be due to the presence of the free carboxylate (COO$^-$) group, which enhances the basic nature of the framework. It is also worthy to mention that when the catalytic reaction was carried out under conventional heating at 80 °C, it achieved a yield of only ca. 20% and 15%, respectively, for the CPs **1** and **2**.

Table 1. Optimization of the parameters of the cascade deacetalization−Knoevenagel condensation reactions between benzaldehyde dimethyl acetal and malononitrile with **1** and **2** as the catalysts [a].

Entry	Catalyst	Time (h)	Amount of Catalyst (mol%)	T (°C)	Solvent	Relative Amount of Unreacted A (%) [b]	Yield of B (%) [b]	Yield of C (%) [b]
1	**1**	4	3	80	Solvent free	7	2	91
2	**2**	4	3	80	Solvent free	10	3	87
3	**1**	0.5	3	80	Solvent free	76	15	9
4	**1**	1	3	80	Solvent free	62	11	27
5	**1**	2	3	80	Solvent free	40	11	49
6	**1**	3	3	80	Solvent free	12	9	79
7	**1**	4	3	80	DMF	21	32	47
8	**1**	4	3	80	THF	46	22	32
9	**1**	4	3	80	DMSO	25	30	45
10	**1**	4	3	80	CH$_3$CN	38	41	21
11	**1**	4	1	80	Solvent free	46	20	34
12	**1**	4	2	80	Solvent free	31	13	56
13	**1**	4	5	80	Solvent free	16	6	78
14	**1**	4	3	25	Solvent free	66	24	10
15	**1**	4	3	50	Solvent free	42	12	46
16	**1**	4	3	100	Solvent free	8	3	89
17	Blank	4	-	80	Solvent free	78	22	0
18	Zn(NO$_3$)$_2$.6H$_2$O	4	3	80	Solvent free	61	32	7
19	**H$_2$L^1**	4	3	80	Solvent free	95	5	0
20	**H$_2$L^2**	4	3	80	Solvent free	96	4	0

[a] Reaction conditions: Benzaldehyde dimethyl acetal (152 mg, 1.0 mmoL) and malononitrile (132 mg, 2.0 mmoL), 3 mol% of catalyst **1** or **2**, 80 °C. [b] Calculated by ^{1}H NMR analysis. **A** = benzaldehyde dimethyl acetal; **B** = benzaldehyde; **C** = benzylidene malononitrile.

We carried out the cascade reaction at different temperatures to examine the effect of temperature. We obtained only 10% of 2-benzylidene malononitrile at room temperature (25 °C) [Table 1, entry 14]. However, increasing the reaction temperature to 50 °C and 80 °C results in a 46% and 91% conversion of benzaldehyde dimethyl acetal into benzylidene malononitrile, respectively (Table 1, entries 15 and 1, respectively). Further increase of temperature to 100 °C had a negative effect on the yield (Table 1, entry 16).

To optimize the catalyst loading, we varied its amount in the range of 1–5 mol% under the above-mentioned experimental conditions. For 1 mol% of catalyst 1 at 80 °C, the yield of 34% of 2-benzylidenemalononitrile was obtained (Table 1, entry 12), whereas upon increasing the catalyst amount to 2 mol% and 3 mol% the final product yield increased to 56% and 91%, respectively (Table 1, entries 12 and 1, respectively). However, a further increase in the catalyst amount to 5 mol% was not favorable (78%, entry 13, Table 1). Thus, the use of 3 mol% of catalyst 1 was considered to provide the best fit for the reaction.

After optimizing the solvent conditions (absence of added solvent), temperature, and catalyst amount, we performed the cascade deacetalization-Knoevenagel condensation reactions at different time intervals. For CP **1**, a time dependent reaction profile illustrating the formation of benzaldehyde (B) and 2-benzylidenemalononitrile with respect to benzaldehyde dimethyl acetal (A) is depicted in Figure 7A. The yield of the final product 2-benzylidenemalononitrile (C) increased up to 4 h, but upon extending the reaction time to 5 h, it was not improved significantly. As shown in Figure 7A, since the onset of the reaction, the amount of benzaldehyde dimethyl acetal (A) persistently diminished with time, consistent with the increasing amount of the benzaldehyde intermediate (B), which reached a maximum at ca. 0.5 h, yielding 2-benzylidenemalononitrile (C) as the final product.
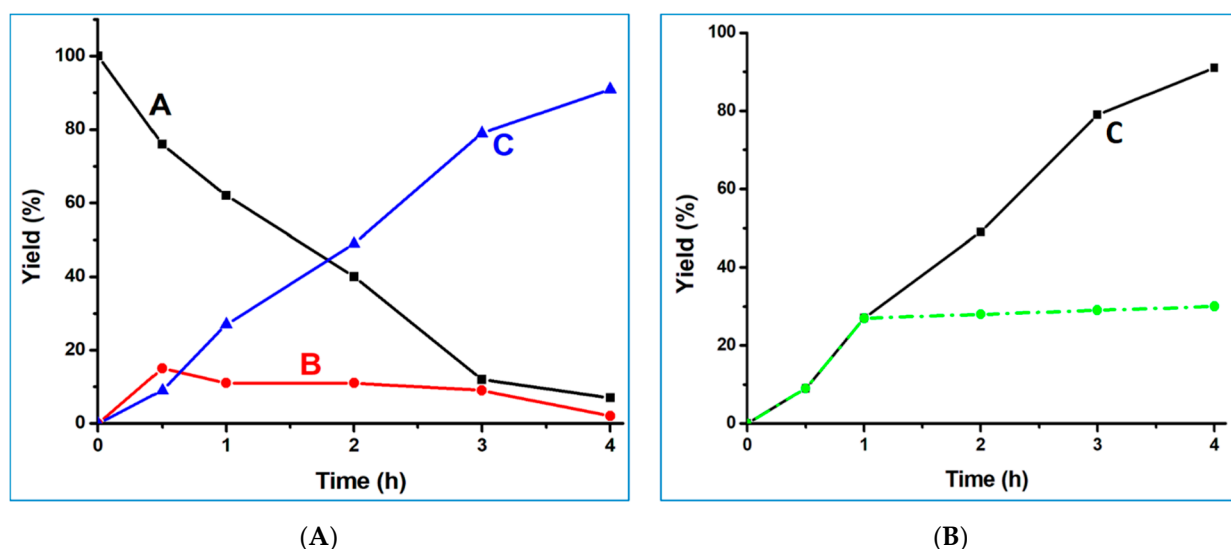

(A)   (B)

Figure 7. (**A**) Plot of yield (or relative amount in case of A) vs. time (h) for the cascade deacetalization-Knoevenagel reactions catalyzed by CP **1** [blue line: 2-benzylidenemalononitrile (C); red line: benzaldehyde (B); black line: unreacted benzaldehyde dimethyl acetal (A)]. (**B**) Plot of yield of C vs. time (h) for the cascade deacetalization-Knoevenagel reactions catalyzed by CP **1** [black line: yield of C); dotted green line: yield of this product upon removal of the catalyst after 1 h of reaction].

Upon performing a blank test (without any catalyst) as well as using the pro-ligands H_2L^1 and H_2L^2 instead of the CP metal catalyst, no 2-benzylidenemalononitrile (C) was formed under the same experimental conditions (Table 1, entries 17, 19, and 20). Moreover, a rather low yield of 2-benzylidenemalononitrile (7%) was observed using the metal salt $Zn(NO_3)_2 \cdot 6H_2O$ as a catalyst (Table 1, entry 18).

To check the recycling behavior, our catalyst 1 was recovered after each run, washed with solvent, and dried again before reuse. It could be reused successively at least three times without having a considerable loss of its catalytic activity (Figure 8). Moreover, to check the heterogeneity of our catalysts, after 1 h of the reaction, the catalyst was removed by centrifugation, and the catalyst-free reaction mixture was left for another 3 h under the optimized conditions. As shown in Figure 7B, an increase in the product yield was not noticed after removing the catalyst (green dotted line), which is consistent with the absence of catalyst leaching and the heterogeneous nature of the catalyst. In addition, we also inspected and compared the structural properties of the catalysts by powder X-ray diffraction analyses before and after the catalytic process (Figures S6 and S7 for CP **1** and **2**, respectively) and the identity of both powder XRD diffractograms supports the structural integrity of the catalyst along with the catalytic reaction.
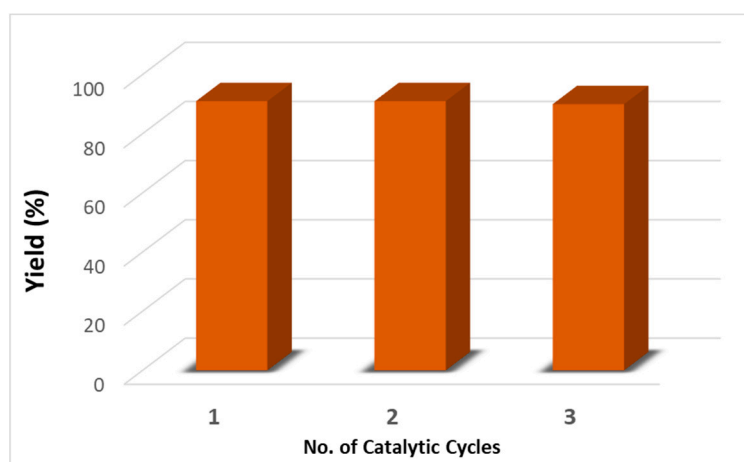

Figure 8. Recyclability of catalyst 1, where the bar represents the yield of 2-benzylidenemalononitrile (C) for the cascade reaction.

A possible reaction mechanism for the one-pot deacetalization-Knoevenagel reaction can be proposed (Figure 9) on the basis of previously published reports [53,54]. In the first reaction, benzaldehyde dimethylacetal is converted to benzaldehyde, a process that is assisted by the acidic catalytic sites. The Lewis acid site further interacts with the carbonyl oxygen of benzaldehyde, making the carbon atom of the C=O bond more susceptible to undergoing nucleophilic attack by deprotanated malononitrile. In fact, the presence of basic sites in the framework leads to the deprotonation of the methylene group of malononitrile, generating the carbanion ion, which attacks the C-atom of the benzaldehyde producing the desired benzylidenemalononitrile, and thereby confirming the synergistic effect of Lewis acid and basic character on the said reaction.

Catalyst 1 was compared with a few other reported Zn(II) based MOFs toward this sort of cascade reaction (Table 2). Although a higher yield was obtained for MOFs $[Zn_2(L')(H_2O)_4]_n \cdot 4n(H_2O)$ (entry 3, Table 2) and $[Zn_4(TBCB)(H_2O)_6]_n.5n(DMAc)$ (entry 4, Table 2), the use of solvent was not avoided in contrast to our system [41,55]. Thus, our catalyst can be claimed as an active one, comparable to those, but operating under better environmentally friendly conditions. It is also noteworthy to mention that the present study provides the first report on Zn(II) based CPs, which act as a heterogeneous catalyst for the above tandem reactions in a solvent-free medium.
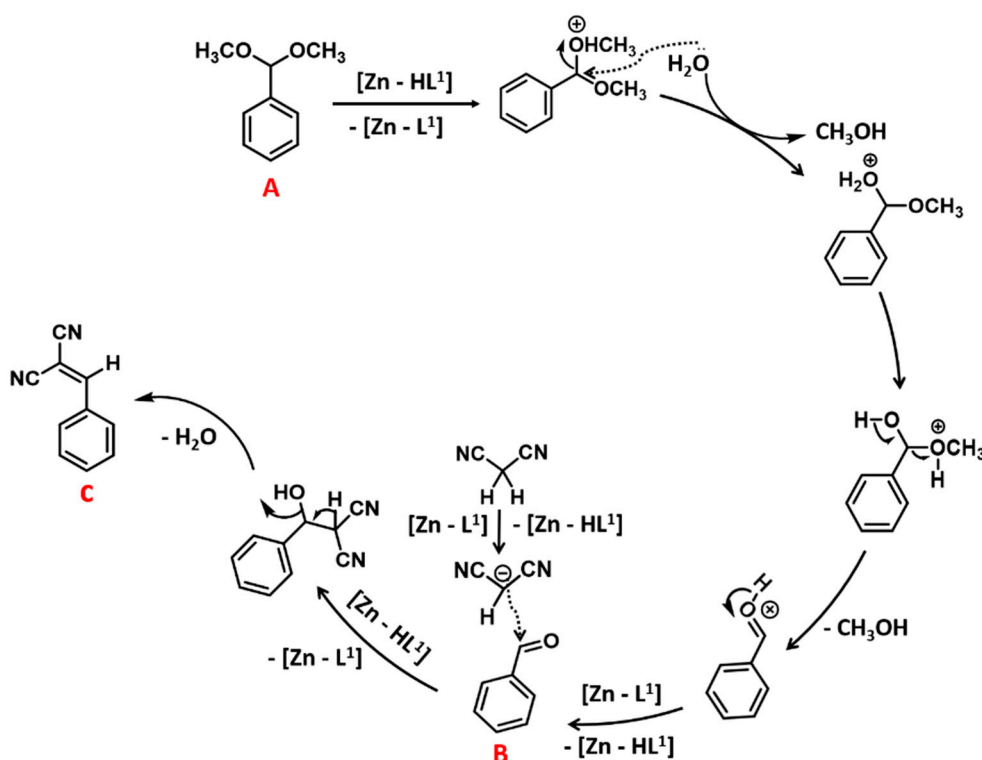
Figure 9. Proposed mechanism for CP **1** catalyzed tandem deacetalization-Knoevenagel condensation. [Zn-L^1] and [Zn-HL^1] denote the unprotonated and a ligand protonated forms of CP **1**. Benzaldehyde dimethyl acetal (A), benzaldehyde (B) and benzylidene malononitrile (C).

Table 2. Comparison of the catalytic activities for one-pot deacetalization-Knoevenagel cascade reactions of a few reported Zn(II) MOFs with our CPs.

Entry	Catalyst	Solvent/Temp/Time	Yield (%)	Ref
1	1	Solvent-free/80 °C/4 h	91	This work
2	2	Solvent-free/80 °C/4 h	87	This work
3	[Zn$_2$(L′)(H$_2$O)$_4$]$_n$·4n(H$_2$O)	DMF/75 °C/3 h	99	41
4	[Zn$_4$(TBCB)(H$_2$O)$_6$]$_n$.5n(DMAc)	1,4-dioxane/90 °C/4 h	99	55

L′: 5, 5′-{(pyridine-2,6-dicarbonyl)bis(azanediyl)}diisophthalate; TBCB: 2,2′,6,6′-tetrakis [3,5-bis-3,5-benzenedicarboxylate]benzidine; DMAc: N,N-dimethylacetamide.

3. Materials and Methods

Methyl 6-hydroxynicotinate, 1,2-dibromoethane, 1,3-dibromopropane, K$_2$CO$_3$, and Zn(NO)$_3$.6H$_2$O (98.0% purity) were obtained from Sigma Aldrich Chemical Co (Lisboa, Portugal). A Bruker Vertex 70 (Bruker Corporation, Ettlingen, Germany) instrument was used for recording the FTIR spectra in KBr pellets. Bruker Avance II + 300 (UltraShield^{TM} Magnet, Rheinstetten, Germany) spectrometers were used for recording the ^{1}H (300 MHz) and ^{13}C (75.45 MHz) NMR, respectively. Elemental analyses (C, H, and N) were performed by the microanalytical service provided by the Instituto Superior Técnico (Lisboa, Portugal). A Bruker APEX-II PHOTON 100 diffractometer was used for collecting the X-ray data with graphite monochromated Mo-Kα (λ = 0.71069) radiation. A D8 Advance Bruker AXS (Bragg Brentano geometry, Bruker, Madison, WI, USA) diffractometer was used for collecting the PXRD data. TGA was carried out under nitrogen atmosphere at a heating rate of 10 °C min^{-1} on a Perkin-Elmer Instrument system (STA6000, Perkin-Elmer, Boston, MA, USA).

3.1. Synthesis and Characterization

3.1.1. Synthesis of 1,1′-(ethane-1,2-diyl)bis(6-oxo-1,6-dihydropyridine-3-carboxylic acid) (H_2L^1)

The pro-ligand H_2L^1 was synthesized in a couple of steps. First, solid K_2CO_3 (0.45 g, 3.27 mmoL) was added to the acetonic solution (40 mL) of methyl 6-hydroxyisonicotinate (0.5 g, 3.26 mmoL) and was stirred for 1 h at RT. To this, 0.14 mL of 1,2-dibromoethane was added dropwise and stirring was continued for another 3 h. The solvent was removed using a rotary evaporator and the white product thus obtained was washed several times with water and air-dried. Yield: 0.35 g (70%). Anal. Calcd. for $C_{16}H_{16}N_2O_6$: C, 57.83; H, 4.85; N, 8.43%. Found: C, 57.10; H, 4.80; N, 8.49%. ^{1}H NMR (DMSO-d_6, δ ppm) 8.27 (s, 2H, Ar-H), 7.72 (d, 2H, Ar-H), 6.36 (d, 2H, Ar-H), 4.31 (s, 4H, -CH$_2$-), 3.89 (s, 6H, -OCH$_3$).

In the subsequent step, the ester form of the pro-ligand was hydrolyzed following a reported protocol to acquire the pro-ligand H_2L^1. Yield: 0.28g (80%). Anal. Calcd for $C_{14}H_{12}N_2O_6$: C, 55.27; H, 3.98; N, 9.21. Found: C, 55.61; H, 3.89; N, 9.26. FT-IR (KBr, cm^{-1}): 1708 (s), 1636 (s), 1584 (s), 1383 (w), 1216 (br), 1143 (s), 851 (w), 778 (w), 609 (s). ^{1}H-NMR (300 MHz, DMSO-d_6, δ ppm): δ 12.81 (s, 2H, COOH), 8.26 (s, 4H, Ar-H), 7.72 (d, 2H, Ar-H), 6.35 (d, 2H, Ar-H), 4.31 (s, 4H, -CH$_2$-). ^{13}C-NMR (77 MHz, DMSO-d_6, δ ppm): 165.79, 162.12, 144.43, 139.24, 119.07, 109.58, 47.22, 29.26. ESI-MS: m/z [(M + H)]$^+$, Calcd. 305.07, found 305.18, [(M + Na)]$^+$, Calcd. 327.07, found 327.89.

3.1.2. Synthesis of 1,1′-(propane-1,3-diyl)bis(6-oxo-1,6-dihydropyridine-3-carboxylic acid) (H_2L^2)

A two-step approach was also utilized for the synthesis of the pro-ligand H_2L^2 as that of H_2L^1. For the preparation of the ester form of the pro-ligand, 1,3-dibromopropane (0.16 mL) was used as a substitute of 1,2-dibromoethane. Yield: 0.32 g (64%). Anal. Calcd for $C_{17}H_{18}N_2O_6$: C, 58.96; H, 5.24; N, 8.09. Found: C, 58.83; H, 5.31; N, 8.14. ^{1}H NMR (DMSO-d_6, δ ppm) 8.49 (s, 2H, Ar-H), 7.75 (d, 2H, Ar-H), 6.48 (d, 2H, Ar-H), 4.01 (s, 4H, -CH$_2$-), 2.02 (s, 2H, -CH$_2$-), 3.89 (s, 6H, -OCH$_3$). In the subsequent step a similar hydrolysis approach was used to yield the pro-ligand H_2L^2. Anal. Calcd for $C_{15}H_{14}N_2O_6$: C, 56.60; H, 4.43; N, 8.80. Found: C, 56.71; H, 4.51; N, 8.82. FT-IR (KBr, cm^{-1}): 1687 (w), 1654 (s), 1531 (s), 1425 (w), 1280 (s), 1122 (s), 934 (w), 745 (s), 630 (s). ^{1}H-NMR (300 MHz, DMSO-d_6, δ ppm): δ 12.81 (s, 2H, COOH), 8.49 (s, 4H, Ar-H), 7.75 (d, 2H, Ar-H), 6.47 (d, 2H, Ar-H), 4.01 (s, 4H, –CH$_2$–), 2.04 (s, 2H, –CH$_2$–). ^{13}C-NMR (77 MHz, DMSO-d_6, δ ppm): 164.89, 161.88, 144.76, 138.95, 119.37, 108.70, 52.18, 47.26, 28.63. ESI-MS: m/z [(M + H)]$^+$, Calcd. 319.09, found 319.63, [(M + Na)]$^+$, Calcd. 341.09, found 341.85.

3.1.3. Synthesis of $[Zn(L^1)(H_2O)_4]_n.nH_2O$ (1)

To a sealed 8 mL glass vessel, an aqueous solution (1 mL) of $Zn(NO_3)_2.6H_2O$ (29 mg, 0.098 mmoL) was added to the previously dissolved H_2L^1 (15 mg, 0.049 mmoL) in 1 mL DMF and was heated at 80 °C for 48 h. White crystals suitable for X-ray diffraction analysis were deposited at the bottom of the glass vial, whereafter they were isolated by sieving and thoroughly washed with deionized DMF and water and air-dried. Yield: 45%. Anal. Calcd for $C_{14}H_{20}N_2O_{11}Zn$: C, 36.73; H, 4.40; N, 6.12. Found: C, 36.81; H, 4.43; N, 6.15. IR (KBr/pellet, cm^{-1}): 2882 (br), 1656 (s), 1562 (s), 1412 (s), 1376 (s), 1330 (w), 1132 (w), 778 (s), 473 (w).

3.1.4. Synthesis of [Zn(L2)(H2O)2]n (2)

A similar approach as that for **1** was utilized, but using H_2L^2 (15 mg, 0.047 mmoL) and $Zn(NO_3)_2.6H_2O$ (28 mg, 0.094 mmoL) in DMF:H_2O (1 mL:1 mL). The white crystals appropriate for X-ray diffraction analysis thus formed were removed by filtration and washed several times with water and DMF and air-dried. Yield: 40%. Anal. Calcd for $C_{15}H_{20}N_2O_{10}Zn$: C, 39.70; H, 4.44; N, 6.17. Found: C, 40.03; H, 4.51; N, 6.25. IR (KBr/pellet, cm^{-1}): 3196 (br), 1637 (s), 1552 (s), 1364 (s), 937 (w), 778 (br), 641 (s), 437 (w).

3.2. Crystal Structure Determination

Single crystal of CPs **1** and **2** suitable for single crystal X-ray diffraction analysis were mounted on a loop and data were collected with a Bruker APEX-II PHOTON 100 diffractometer (graphite Mo-Kα, 0.71069 wavelength radiation) at 150 K for **1** and at room temperature for **2**. Phi and omega scans were utilized for acquiring the full sphere of data at a scan of 0.5° per frame. Bruker SMART software was used for retrieving the cell parameters and the refinement was done using Bruker SAINT [56]. SADABS [57] was applied for the absorption corrections. Structures were solved by direct methods using the SHELXS-2014 package and further refinements were done using SHELXL-2014/6 [58]. WinGX System-Version 2014.1 [59] was used to perform the calculations. The H-atoms on C and N were included at geometrically calculated settings and refined using the riding-model approximation. All atoms (except hydrogens) were refined anisotropically. The disordered water molecules in 1 were modeled by means of the PART instruction. Those in 2, however, could not be modeled reliably and PLATON/SQUEEZE [60] was applied to correct the data. A volume of 184 Å^3 with 63 electrons per unit cell was obtained, fitting well for two water molecules in the asymmetric unit, which were included in the empirical formula for the final refinement. The water content in the void was supported by elemental and thermogravimetric analyses. Crystallographic data for CPs **1** and **2** are presented in Table S1 (Supplementary Materials) and important bond distances and angles are given in Table S2. CCDC 2051303-2051304 contains the supplementary crystallographic data for this paper. These data can be obtained free of charge from The Cambridge Crystallographic Data Center via www.ccdc.cam.ac.uk/data_request/cif.

4. Conclusions

We synthesized and characterized two new 1D Zn(II) CPs, $[Zn(L^1)(H_2O)_4]_n \cdot n(H_2O)$ (**1**) and $[Zn(L^2)(H_2O)_2]_n$ (**2**) with two new flexible dicaboxylate ligands. The structural aspects of both CPs **1** and **2** were disclosed and authenticated by single-crystal X-ray diffraction analysis. The underlying topology of the CPs was illustrated by the topological analysis of H-bonded structure of CP **1**, which revealed a 3,4,6-connected trinodal net and point symbol. On the other hand, topological analysis of the hydrogen-bonded network of CP **2** disclosed a 2,3,3,4,6,7-connected hexanodal net.

These CPs act as heterogeneous catalysts for the one-pot tandem deacetalization–Knoevenagel condensation reactions under environmentally friendly conditions. Both of them exhibited a good product yield of ca. 91 and 87% in solvent-free medium under microwave-assisted conditions. To our knowledge, these are the first Zn(II) based CPs to be applied as heterogeneous catalysts for the microwave-assisted one-pot tandem deacetalization–Knoevenagel condensation reactions under environmentally friendly conditions. The recyclability of catalysts 1 was also evaluated, showing that it can be used up to three cycles without losing its activity.

This study shows the relevance of flexible dicarboxylate ligands with both Lewis acidic and basic sites on the catalytic behavior of Zn(II) CPs for the tandem deacetalization–Knoevenagel condensation reactions. Further research on the architectural and rational design of new CPs/MOFs, based on different metals, using a ligand system with the properties for such a type of catalytic systems, is worthy of being explored.

Author Contributions: A.P.: Conceptualization, investigation, formal analysis, project administration, catalysis, writing original draft, review and editing; A.K.: catalytic studies and manuscript writing; M.F.C.G.d.S.: performed X-ray analysis, writing-review and editing; A.J.L.P.: writing—review, editing and correction. All authors have read and agreed to the published version of the manuscript.

Institutional Review Board Statement: Not applicable.

Informed Consent Statement: Not applicable.

Conflicts of Interest: The authors declare no conflict of interest.

References

1. Ghasempour, H.; Wang, K.Y.; Powell, J.A.; ZareKarizi, F.; Lv, X.L.; Morsali, A.; Zhou, H.C. Metal–organic frameworks based on multicarboxylate linkers. *Coord. Chem. Rev.* **2021**, *426*, 213542. [CrossRef]

2. Kumar, N.; Wang, S.Q.; Mukherjee, S.; Bezrukov, A.A.; Patyk-Kaźmierczak, E.; O'Nolan, D.; Kumar, A.; Yu, M.H.; Chang, Z.; Bu, X.H.; et al. Crystal engineering of a rectangular sql coordination network to enable xylenes selectivity over ethylbenzene. *Chem. Sci.* **2020**, *11*, 6889–6895. [CrossRef] [PubMed]

3. Yue, Q.; Gao, E.Q. Azide and carboxylate as simultaneous coupler for magnetic coordination polymers. *Coord. Chem. Rev.* **2019**, *382*, 1–31. [CrossRef]

4. Wang, S.D.; Xie, L.X.; Zhao, Y.F.; Wang, Y.N. A dual luminescent sensor coordination polymer for simultaneous determination of ascorbic acid and tryptophan. *Spectrochim. Acta Part A Mol. Biomol. Spectrosc.* **2020**, *242*, 118750. [CrossRef]

5. Paul, A.; Das, K.; Karmakar, A.; Guedes Da Silva, M.F.C.; Pombeiro, A.J.L. A mechanistic insight into the rapid and selective removal of Congo Red by an amide functionalised Zn(ii) coordination polymer. *Dalton Trans.* **2020**, *49*, 12970–12984. [CrossRef]

6. Tu, Q.Q.; Ren, L.L.; Cui, Y.Y.; Cheng, A.L.; Gao, E.Q. Assembly of four new cobalt coordination polymers modulated by N-coligands: Sensitive and selective sensing of nitroaromatics, Fe^{3+} and $Cr_2O_7^{2-}$ in water. *CrystEngComm* **2020**, *22*, 1789–1801. [CrossRef]

7. Li, B.; Yan, Q.Q.; Yong, G.P. A new porous coordination polymer reveals selective sensing of Fe^{3+}, $Cr_2O_7^{2-}$, CrO_4^{2-}, MnO_4^- and nitrobenzene, and stimuli-responsive luminescence color conversions. *J. Mater. Chem. C* **2020**, *8*, 11786–11795. [CrossRef]

8. Biradha, K.; Goswami, A.; Moi, R. Coordination polymers as heterogeneous catalysts in hydrogen evolution and oxygen evolution reactions. *Chem. Commun.* **2020**, *56*, 10824–10842. [CrossRef]

9. Wang, J.; Qi, T.; Li, Z.; She, W.; Li, X.; Li, J.; Yan, P.; Li, W.; Li, G. A strategy of two-step tandem catalysis towards direct N-alkylation of nitroarenes with ethanol via facile fabricated novel Co-based catalysts derived from coordination polymers. *J. Catal.* **2019**, *376*, 106–118. [CrossRef]

10. Bhaskaran; Trivedi, M.; Yadav, A.K.; Singh, G.; Kumar, A.; Kumar, G.; Husain, A.; Rath, N.P. Synthetic, spectral, structural and catalytic activity of infinite 3-D and 2-D copper(ii) coordination polymers for substrate size-dependent catalysis for CO_2 conversion. *Dalton Trans.* **2019**, *48*, 10078–10088. [CrossRef]

11. Gu, J.; Wen, M.; Cai, Y.; Shi, Z.; Nesterov, D.S.; Kirillova, M.V.; Kirillov, A.M. Cobalt(II) Coordination Polymers Assembled from Unexplored Pyridine-Carboxylic Acids: Structural Diversity and Catalytic Oxidation of Alcohols. *Inorg. Chem.* **2019**, *58*, 5875–5885. [CrossRef]

12. Markad, D.; Khullar, S.; Mandal, S.K. Engineering a Nanoscale Primary Amide-Functionalized 2D Coordination Polymer as an Efficient and Recyclable Heterogeneous Catalyst for the Knoevenagel Condensation Reaction. *ACS Appl. Nano Mater.* **2018**, *1*, 5226–5236. [CrossRef]

13. Karmakar, A.; Pombeiro, A.J.L. Recent advances in amide functionalized metal organic frameworks for heterogeneous catalytic applications. *Coord. Chem. Rev.* **2019**, *395*, 86–129. [CrossRef]

14. Banerjee, D.; Finkelstein, J.; Smirnov, A.; Forster, P.M.; Borkowski, L.A.; Teat, S.J.; Parise, J.B. Synthesis and structural characterization of magnesium based coordination networks in different solvents. *Cryst. Growth Des.* **2011**, *11*, 2572–2579. [CrossRef]

15. Chen, J.; Ohba, M.; Zhao, D.; Kaneko, W.; Kitagawa, S. Polynuclear core-based nickel 1,4-cyclohexanedicarboxylate coordination polymers as temperature-dependent hydrothermal reaction products. *Cryst. Growth Des.* **2006**, *6*, 664–668. [CrossRef]

16. Wang, J.K.; Wang, X.W.; Wang, Z.S.; Yao, L.S.; Niu, L.Z.; Yu, Y.H.; Gao, J.S. Two zinc coordination polymers constructed by 4′-hydroxy-[1,1′-biphenyl]-3,5-dicarboxylic acid (H_2BDA) and 4-hydroxy-[1,1′-biphenyl]-3,3′,5,5′-tetracarboxylic acid (H_3BTA): Synthesis, structures and luminescence identifying properties. *Polyhedron* **2019**, *167*, 85–92. [CrossRef]

17. Sahu, J.; Ahmad, M.; Bharadwaj, P.K. Structural diversity and luminescence properties of coordination polymers built with a rigid linear dicarboxylate and Zn(II)/Pb(II) ion. *Cryst. Growth Des.* **2013**, *13*, 2618–2627. [CrossRef]

18. Karra, J.R.; Huang, Y.G.; Walton, K.S. Synthesis, characterization, and adsorption studies of nickel(II), zinc(II), and magnesium(II) coordination frameworks of BTTB. *Cryst. Growth Des.* **2013**, *13*, 1075–1081. [CrossRef]

19. Zheng, S.L.; Yang, J.H.; Yu, X.L.; Chen, X.M.; Wong, W.T. Syntheses, Structures, Photoluminescence, and Theoretical Studies of d 10 Metal Complexes of 2,2′-Dihydroxy-[1,1′]binaphthalenyl-3,3′-dicarboxylate. *Inorg. Chem.* **2004**, *43*, 830–838. [CrossRef]

20. Feng, L.; Wang, K.Y.; Yan, T.H.; Zhou, H.C. Seed-mediated evolution of hierarchical metal-organic framework quaternary superstructures. *Chem. Sci.* **2020**, *11*, 1643–1648. [CrossRef]

21. Chainok, K.; Ponjan, N.; Theppitak, C.; Khemthong, P.; Kielar, F.; Dungkaew, W.; Zhou, Y.; Batten, S.R. Temperature-dependent 3D structures of lanthanide coordination polymers based on dicarboxylate mixed ligands. *CrystEngComm* **2018**, *20*, 7446–7457. [CrossRef]

22. Chen, M.; Hu, M.; Zhao, H.; Tian, J.Y.; Liu, C. Sen Solvent-Controlled Construction of Two 3D Manganese(II) Coordination Polymers Based on Flexible Tripodal Multicarboxylate Linker and Rod-Shaped SBUs. *Zeitschrift Anorg. Allg. Chem.* **2016**, *642*, 778–784. [CrossRef]

23. Xiong, G.; Wang, Y.; Zhao, B.; You, L.; Ren, B.; He, Y.; Wang, S.; Sun, Y. Temperature-tuned topologies and interpenetrations of two 3D porous copper(II)-organic frameworks and gas adsorption behaviors. *Inorganica Chim. Acta* **2018**, *471*, 180–185. [CrossRef]

24. Jarrah, N.; Troyano, J.; Carné-Sánchez, A.; Imaz, I.; Tangestaninejad, S.; Moghadam, M.; Maspoch, D. Dynamic porous coordination polymers built-up from flexible 4,4′-dithiodibenzoate and rigid N-based ligands. *Dalton Trans.* **2020**, *49*, 13142–13151. [CrossRef]

25. Nandi, S.; De Luna, P.; Maity, R.; Chakraborty, D.; Daff, T.; Burns, T.; Woo, T.K.; Vaidhyanathan, R. Imparting gas selective and pressure dependent porosity into a non-porous solid: Via coordination flexibility. *Mater. Horiz.* **2019**, *6*, 1883–1891. [CrossRef]

26. Hawes, C.S.; Chilton, N.F.; Moubaraki, B.; Knowles, G.P.; Chaffee, A.L.; Murray, K.S.; Batten, S.R.; Turner, D.R. Coordination polymers from a highly flexible alkyldiamine-derived ligand: Structure, magnetism and gas adsorption studies. *Dalton Trans.* **2015**, *44*, 17494–17507. [CrossRef]

27. Guo, H.; Guo, X.; Zou, H.; Qi, Y.; Chen, R.; Zhao, L.; Liu, C. A series of coordination polymers assembled from 9,9-dimethylfluorene-2,7- dicarboxylic acid and various flexible bis(imidazole) ligands: Synthesis, structures and properties. *CrystEngComm* **2014**, *16*, 7459–7468. [CrossRef]

28. Colón, Y.J.; Furukawa, S. Understanding the role of linker flexibility in soft porous coordination polymers. *Mol. Syst. Des. Eng.* **2020**, *5*, 284–293. [CrossRef]

29. Kim, H.C.; Huh, S.; Kim, J.Y.; Moon, H.R.; Lee, D.N.; Kim, Y. Zn-MOFs containing flexible α,ω-alkane (or alkene)-dicarboxylates with 1,2-bis(4-pyridyl)ethylene: Comparison with Zn-MOFs containing 1,2-bis(4-pyridyl)ethane ligands. *CrystEngComm* **2017**, *19*, 99–109. [CrossRef]

30. Hwang, I.H.; Kim, H.Y.; Lee, M.M.; Na, Y.J.; Kim, J.H.; Kim, H.C.; Kim, C.; Huh, S.; Kim, Y.; Kim, S.J. Zn-MOFs containing flexible α,ω-alkane (or alkene)- dicarboxylates and 1,2-bis(4-pyridyl)ethane ligands: CO_2 sorption and photoluminescence. *Cryst. Growth Des.* **2013**, *13*, 4815–4823. [CrossRef]

31. Ma, L.; Wu, H.; Yang, J.; Liu, Y.Y.; Ma, J.F. Syntheses, crystal structures and knoevenagel condensation reactions of three coordination polymers assembled with Lewis basic ligand. *Polyhedron* **2018**, *144*, 6–10. [CrossRef]

32. Gupta, M.; De, D.; Pal, S.; Pal, T.K.; Tomar, K. A porous two-dimensional Zn(II)-coordination polymer exhibiting SC-SC transmetalation with Cu(II): Efficient heterogeneous catalysis for the Henry reaction and detection of nitro explosives. *Dalton Trans.* **2017**, *46*, 7619–7627. [CrossRef] [PubMed]

33. Huang, C.; Wang, H.; Wang, X.; Gao, K.; Wu, J.; Hou, H.; Fan, Y. Surfactant-Assisted Nanocrystalline Zinc Coordination Polymers: Controlled Particle Sizes and Synergistic Effects in Catalysis. *Chem. A Eur. J.* **2016**, *22*, 6389–6396. [CrossRef] [PubMed]

34. Xue, L.P.; Li, Z.H.; Zhang, T.; Cui, J.J.; Gao, Y.; Yao, J.X. Construction of two Zn(ii)/Cd(ii) multifunctional coordination polymers with mixed ligands for catalytic and sensing properties. *New J. Chem.* **2018**, *42*, 14203–14209. [CrossRef]

35. Manuscript, A.; Society, R.; Manuscripts, A.; Manuscript, T.A.; Manuscripts, A.; Society, R.; Manuscript, A. Amide Functionalized Metal Organic Frameworks for Diastereoselective Nitroaldol (Henry) Reaction in Aqueous Medium. *RSC Adv.* **2015**, *5*, 87400–87410.

36. Paul, A.; Martins, L.M.D.R.S.; Karmakar, A.; Kuznetsov, M.L.; Novikov, A.S.; Guedes da Silva, M.F.C.; Pombeiro, A.J.L. Environmentally benign benzyl alcohol oxidation and C-C coupling catalysed by amide functionalized 3D Co(II) and Zn(II) metal organic frameworks. *J. Catal.* **2020**, *385*, 324–337. [CrossRef]

37. Karmakar, A.; Guedes Da Silva, M.F.C.; Pombeiro, A.J.L. Zinc metal-organic frameworks: Efficient catalysts for the diastereoselective Henry reaction and transesterification. *Dalton Trans.* **2014**, *43*, 7795–7810. [CrossRef]

38. Karmakar, A.; Guedes Da Silva, M.F.C.; Hazra, S.; Pombeiro, A.J.L. Zinc amidoisophthalate complexes and their catalytic application in the diastereoselective Henry reaction. *New J. Chem.* **2015**, *39*, 3004–3014. [CrossRef]

39. Dhakshinamoorthy, A.; Garcia, H. Cascade Reactions Catalyzed by Metal Organic Frameworks. *ChemSusChem* **2014**, *7*, 2392–2410. [CrossRef]

40. Huang, Y.B.; Liang, J.; Wang, X.S.; Cao, R. Multifunctional metal-organic framework catalysts: Synergistic catalysis and tandem reactions. *Chem. Soc. Rev.* **2017**, *46*, 126–157. [CrossRef]

41. Karmakar, A.; Paul, A.; Rúbio, G.M.D.M.; Soliman, M.M.A.; Guedes da Silva, M.F.C.; Pombeiro, A.J.L. Highly Efficient Bifunctional Amide Functionalized Zn and Cd Metal Organic Frameworks for One-Pot Cascade Deacetalization–Knoevenagel Reactions. *Front. Chem.* **2019**, *7*, 1–10. [CrossRef] [PubMed]

42. Karmakar, A.; Soliman, M.M.A.; Rúbio, G.M.D.M.; Guedes Da Silva, M.F.C.; Pombeiro, A.J.L. Synthesis and catalytic activities of a Zn(ii) based metallomacrocycle and a metal-organic framework towards one-pot deacetalization-Knoevenagel tandem reactions under different strategies: A comparative study. *Dalton Trans.* **2020**, *49*, 8075–8085. [CrossRef] [PubMed]

43. Toyao, T.; Fujiwaki, M.; Horiuchi, Y.; Matsuoka, M. Application of an amino-functionalised metal-organic framework: An approach to a one-pot acid-base reaction. *RSC Adv.* **2013**, *3*, 21582–21587. [CrossRef]

44. Chen, Y.Z.; Zhou, Y.X.; Wang, H.; Lu, J.; Uchida, T.; Xu, Q.; Yu, S.H.; Jiang, H.L. Multifunctional PdAg@MIL-101 for One-Pot Cascade Reactions: Combination of Host-Guest Cooperation and Bimetallic Synergy in Catalysis. *ACS Catal.* **2015**, *5*, 2062–2069. [CrossRef]
45. Liu, H.; Xi, F.G.; Sun, W.; Yang, N.N.; Gao, E.Q. Amino- and sulfo-bifunctionalized metal-organic frameworks: One-pot tandem catalysis and the catalytic sites. *Inorg. Chem.* **2016**, *55*, 5753–5755. [CrossRef]
46. Mistry, S.; Sarkar, A.; Natarajan, S. New Bifunctional Metal-Organic Frameworks and Their Utilization in One-Pot Tandem Catalytic Reactions. *Cryst. Growth Des.* **2019**, *19*, 747–755. [CrossRef]
47. Yaghi, M.O. *Reticular Chemistry Structure Resource*; Arizona State University: Tempe, AZ, USA, 2005; Available online: Http://rcsr.anu.edu.au/ (accessed on 18 December 2020).
48. Blatov, V.A. Multipurpose crystallochemical analysis with the program package TOPOS. *IUCr Comput. Comm. Newslett.* **2006**, *7*, 4. Available online: http://www.topos.ssu.samara (accessed on 18 December 2020).
49. Blatov, V.A. Nanocluster analysis of intermetallic structures with the program package TOPOS. *Struct. Chem.* **2012**, *23*, 955–963. [CrossRef]
50. Paul, A.; Martins, L.M.D.R.S.; Karmakar, A.; Kuznetsov, M.L.; da Silva, M.F.C.G.; Pombeiro, A.J.L. Zn(II)-to-Cu(II) Transmetalation in an Amide Functionalized Complex and Catalytic Applications in Styrene Oxidation and Nitroaldol Coupling. *Molecules* **2020**, *25*, 2644. [CrossRef]
51. Polshettiwar, V.; Varma, R.S. Microwave-assisted organic synthesis and transformations using benign reaction media. *Acc. Chem. Res.* **2008**, *41*, 629–639. [CrossRef]
52. Rathi, A.K.; Gawande, M.B.; Zboril, R.; Varma, R.S. Microwave-assisted synthesis—Catalytic applications in aqueous media. *Coord. Chem. Rev.* **2015**, *291*, 68–94. [CrossRef]
53. Mu, M.; Yan, X.; Li, Y.; Chen, L. Post-modified acid-base bifunctional MIL-101(Cr) for one-pot deacetalization-Knoevenagel reaction. *J. Nanoparticle Res.* **2017**, *19*, 148. [CrossRef]
54. Zheng, M.; Wang, Y.; Feng, P. Bifunctional heterometallic metal-organic frameworks for solvent-free heterogeneous cascade catalysis. *Catalysts* **2020**, *10*, 309. [CrossRef]
55. He, H.; Sun, F.; Aguila, B.; Perman, J.A.; Ma, S.; Zhu, G. A bifunctional metal—Organic framework featuring the combination of open metal sites and Lewis basic sites for selective gas adsorption and heterogeneous cascade catalysis. *J. Mater. Chem. A* **2016**, *4*, 15240–15246. [CrossRef]
56. RSC Advances. *Bruker, APEX2*; Bruker AXS Inc.: Madison, WI, USA, 2012.
57. Sheldrick, G.M. *SADABS, Program for Empirical Absorption Correction of Area Detector Data*; University of Gottingen: Gottingen, Germany, 1996.
58. Sheldrick, G.M. Crystal structure refinement with SHELXL. *Acta Crystallogr.* **2015**, *C71*, 3–8.
59. Farrugia, L.J. WinGX and ORTEP for Windows: An update. *J. Appl. Crystallogr.* **2012**, *45*, 849–854. [CrossRef]
60. Spek, A.L. Structure validation in chemical crystallography. *Acta Crystallogr. Sect. D Biol. Crystallogr.* **2009**, *65*, 148–155. [CrossRef]